Nanoparticle Adsorption on a Weak Polyelectrolyte. Stiffness, pH, Charge Mobility, and Ionic Concentration Effects Investigated by Monte Carlo Simulations

Serge Ulrich, Marianne Seijo, Abohachem Laguecir, and Serge Stoll*

Department of Inorganic, Analytical and Applied Chemistry, University of Geneva, Sciences II, 30 Quai E. Ansermet, CH-1211 Geneva 4, Switzerland

Received: June 13, 2006; In Final Form: August 15, 2006

Monte Carlo simulations have been used to study two different models for a weak linear polyelectrolyte in the presence of nanoparticles: (i) a rodlike and (ii) a flexible polyelectrolytes. The use of simulated annealing has made it possible to simulate a polyelectrolyte chain in the presence of several nanoparticles by improving conformation sampling and avoiding multiple minima problems when dense conformations are produced. Nanoparticle distributions along the polymer backbone were analyzed versus the ionic concentration, polyelectrolyte stiffness, and nanoparticle surface charge. Titration curves were calculated and the influences of the ionic concentration, solution pH, and number of adsorbed nanoparticles on the acid/base polyelectrolyte properties have been systematically investigated. The subtle balance of attractive and repulsive interactions has been discussed, and some characteristic conformations are presented. The comparison of the two limit models provides a good representation of the stiffness influence on the complex formation. In some conditions, overcharging was obtained and presented with respect to both the polyelectrolyte and nanoparticle as the central element. Finally, the charge mobility influence along the polyelectrolyte backbone was investigated by considering annealed and quenched polyelectrolyte chains.

I. Introduction

The term polyelectrolyte (PE) denotes generally charged macromolecules carrying acidic or basic monomers.[1,2] Under appropriate conditions, monomers dissociate and positively or negatively charges are created along the chain. The PE is defined as s*trong* when the charge distribution along the PE only depends on its initial chemistry and remains fixed over a wide range of solution pH, whereas it is defined as *weak* when the charge distribution is sensible to pH variations. Hence in the case of weak PEs, conformational changes are depending on parameters such as ionic concentration, solution pH, and PE concentration.

Several theories and experiences have been proposed to explain the potentiometric titration of weak PEs in aqueous solutions.[3−10] The dissociation of an isolated acid monomer (HA) in an aqueous medium is given by $HA \rightleftharpoons H^+ + A^-$. According to the mass action law, the equilibrium constant is

$$K_0 = \frac{[H^+][A^-]}{[HA]} \quad (1)$$

where $[H^+]$, $[A^-]$, and $[HA]$ are the concentrations of dissociated hydrogen and dissociated and undissociated acid, respectively. The degree of ionization α is then defined by

$$\alpha = \frac{[A^-]}{[A^-] + [HA]} \quad (2)$$

In agreement with experimental observations, the continuous increase of the apparent pK of a polymeric acid with increasing α is usually observed. This effect is due to the increasing difficulty to remove protons with the increase of α because of the increasing of electrostatic repulsions between the charged monomers. Thus, one can define

$$\Delta pK = pK - pK_0 = pH - pK_0 + \log[(1 - \alpha)/\alpha] \quad (3)$$

as the shift between the apparent negative logarithm of the dissociation constant and the negative logarithm of the dissociation constant of an ideal monomer solution, pK_0, in absence of electrostatic interactions.

PE complexation with nanoparticles (NPs) is located at the interface of several disciplines and represents an important issue because of key applications in drug delivery device,[11,12] nanotoxicology,[13−15] and water treatment.[16−18] In particular, magnetic NPs are nowadays attracting much interest as a labeling material in the fields of medical applications as biologically active systems and magnetic resonance imaging just to quote a few.[19] The surface modification of NPs by macromolecules such as ligands and polymers is also important for their functionalization to reach a target or to deliver a drug to a specific location and to increase the residence time of the NPs in body fluids.[20] In water treatment, flocculation acts as one of the key physicochemical regulation processes of trace compounds. Floc formation is expected to occur between mineral NPs and natural polymers and are eliminated from the water column by sedimentation.[21] The ability of natural or synthetic PEs to adsorb and adhere to the NP surface and also the final conformation of the complex are expected to control the structure/activity relationship in drug design and stabilization/destabilization of PE and NP mixtures.

Complexation depends on factors such as pH, ionic concentration, and mixing ratio, in addition to intrinsic factors related

* To whom correspondence should be addressed. E-mail: serge.stoll@cabe.unige.ch.

Nanoparticle Adsorption on a Polyelectrolyte

J. Phys. Chem. B, Vol. 110, No. 42, 2006 **20955**

to the chemical composition of the species, chain stiffness, and relative sizes of PEs and NPs. In two different papers,[22,23] Dubin and co-workers reviewed recent developments and foundations in the general subject of protein/PE complexes and investigated experimentally the complexation of PEs to oppositely charged dendrimers[24−29] or proteins.[30−32] They pointed out the importance of the surface charge density in controlling the adsorption/desorption limits which were found proportional to the inverse Debye screening length.

Berret and co-workers investigated the complexation between PEs and ionic surfactant micelles and inorganic oxide NPs. They considered both linear and comb architectures, designed novel core−shell nanostructures, and confirmed that their formation was electrostatic self-assembled.[20,33] They also produced cerium NPs irreversibly coated with poly(acrylic acid) chains by a precipitation/redispersion process.[34] The complexes were stable over a wide range of pH and concentration.

Ilekti and co-workers[35] presented experimental results on the effects of PEs on surfactant aggregates by means of small-angle X-ray scattering. The authors considered a mixture of sodium polyacrylate and dilute micellar solution of cetyltrimethylammonium bromide. When PEs were added to the dilute micellar solution, the micelles were stuck together by polyion bridges in a concentrated phase.

PE/NP complexes have motivated a great amount of analytical approaches.[36−45] Von Goeler and Muthukumar[36] investigated theoretically the influence of PE charge density on adsorption processes at spherical and cylindrical surfaces. They shown that complexation largely depends on ionic concentration and temperature. A critical temperature T_c was considered and found to depend on parameters such as the molecular weight of the polymer, the ionic concentration, and surface curvature. When $T > T_c$, complexation was not observed, whereas the PE was fully adsorbed when $T < T_c$. Also considering planar or spherical surfaces, Muthukumar established the critical conditions necessary for adsorption of uniformly charged PE as well as the kinetics of the adsorption process.[37]

Netz and Joanny theoretically provided a full complexation phase diagram for a semiflexible PE in the presence of an oppositely charged sphere.[42,43] They demonstrated that for intermediate salt concentration and high sphere charge, a strongly bound complex, where the PE completely wraps around the sphere, is obtained. On the other hand, the low salt regime was dominated by monomer/monomer repulsions leading to a conformation where some monomers are distributed in tails. In the high salt regime, the authors suggested that the polymer partially wraps the sphere. More recently, Boroudjerdi and Netz reviewed the complexation of a semiflexible PE with an oppositely charged particle using parameters fitting the DNA/histone system.[46] To understand the properties of complexes in solution, the interactions between two complexes were considered. The authors presented the corresponding phase diagram as a function of the separation distance of the two complexes and the inverse Debye screening length κ: They distinguished a phase where both complexes present the same structure (symmetric phase) from an other phase (asymmetric phase) where the complexes exhibit different structures because mutual interactions. The asymmetric phase had several conformations, and as a result, a third phase was also put in evidence where one of the two chains was simultaneously adsorbed on both spheres (bridging phase).

Recently, the binding affinity of PEs for both the bovine serum albumin protein and an oppositely charged micelle was experimentally investigated.[47] Here, computer simulations were used with the goal of interpreting experimental data and clarifying the importance of charge mobility and charge density on the complexation. Since computer simulations represent a successful tool to support both theory and experiments, a wide number of simulations reported in the literature have focused on the complexation of one strong PE with one NP[48−53] or several NPs.[39,54−56] Complexation between a strong PE and many spherical NPs were studied with a primitive model by means of Monte Carlo (MC) simulations by Skepö and Linse.[54−56] The authors considered different systems with combinations of two chain lengths (N_m = 20 or 40) and two different NPs charges (Z_{np} = −10e or −20e). Among others, Skepö and Linse investigated the dissolution of a PE/NPs complex by addition of salt.[56]

Stoll and co-workers used MC simulations to study the interactions between a charged micelle and a flexible chain[57] according to a well-defined experimental system initially investigated by Dubin and co-workers.[27] The authors demonstrated that the complexation process leads to a multitude of possible structures ranging from collapsed to tangent conformations. The adsorption/desorption limits found by MC simulations with respect to the charge density of the micelle and the salt concentration were in good agreement with the experimental data.[27] The effects of the micelle concentration were also investigated, and it was found that the adsorption limit is moved to higher ionic strengths for the more concentrated systems.

Suspecting the importance of solution pH and PE acid/base properties, in previous contributions,[8,9] we investigated the complex formation between a weak PE and one spherical oppositely charged NP using a Monte Carlo approach. Titration curves clearly demonstrated that the acid/base properties of the PE were largely depending on the NP surface charge density σ and ionic concentration C_i. Considering intrinsic flexible chains,[8] fully charged PEs totally wrap around the NP or partially wrap around the NP with a large tail in solution. An increase of the possible conformations such as "U", solenoid, or rosette conformations was observed with semiflexible chains at different ionic concentrations.[9] We also pointed out that if chain stiffness promotes PE expansion and ionization, it penalizes PE adsorption at the NP surface owing to the decrease of the number of monomers in trains, i.e., directly in contact with the NP surface.

Complexation of a charged spherical NP by an oppositely charged PE can, in some conditions, induce charge inversion. This effect termed as *overcharging* has attracted significant attention and has been investigated by analytical models. Mateescu and co-workers found using simulations that the overcharging is promoted with increasing the size of the NPs[38] whereas Nguyen and Shklovskii predicted an increase of charge inversion with the increase of the ionic concentration and NP size.[41]

The main purpose of the present study is to extend the model to systems involving several NPs and by considering an oppositely charged weak PE. We particularly focus on the dissolution of complexes formed by PE and NPs by adjusting of the solution pH and ionic concentration. For the sake of clarity, two models are introduced (Figure 1): (i) a rodlike (model 1) and (ii) a flexible PE (model 2). Both synthetic and biomacromolecules can exhibit rodlike PE conformations, for example, poly(p-phenylene) (PPP) owing to the linear configuration of the phenylene repeat units[58] and rigid biopolymers released from plankton as exudates or cell wall components (such as succinoglycan) which are found in aquatic systems.[59] Stiffness influence follows from comparisons of these two models.

model 1

$N_m = 200$
$\alpha = 0.70$

model 2
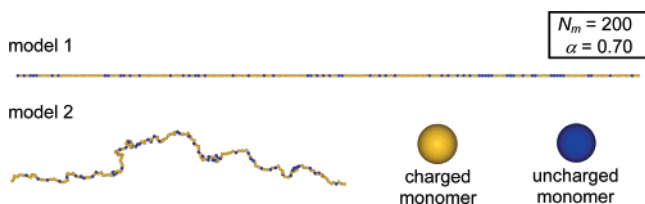
charged monomer   uncharged monomer

Figure 1. Model 1 consists of a rodlike chain whereas model 2 is a flexible chain. The bond length between monomers is constant (7.14 Å), and the number of monomer is set to $N_m = 200$ in all simulations. The rodlike polyelectrolyte cannot change its conformation during simulations. Charged monomers are represented by yellow spheres, whereas noncharged monomers are represented by blue spheres. The degree of ionization α was here chosen arbitrarily and set to $\alpha = 0.70$.

The paper is organized as follows: first, Monte Carlo procedures and models are presented. When flexible or semiflexible PE is considered, the use of simulated annealing to improve the conformational sampling is discussed. Then the roles of ionic concentration and NP surface charge densities are systematically investigated in both models and chain conformations are characterized. Special attention is given to the overcharging phenomenon during titration with the perspective of under- and overcharging situations depending on the entity under consideration.

II. Models

One linear PE is simulated with the assumption of a very dilute solution. The PE chain is represented as N_m jointed hard spheres to take into account the excluded volume effect. The number of monomers is set to $N_m = 200$. To avoid the domain of the Manning counterion condensation,[60] each sphere is considered to be a physical monomer of radius $R_m = l_B/2 = 3.57$ Å, where l_B represents the Bjerrum length at 298 K. Each monomer is a titrating site that can either carry a charge $z_m = -1$ on its center or be uncharged. As previously discussed, two different PE models have been considered (Figure 1): model 1 is a strictly linear PE, i.e., a rodlike PE whereas, model 2 is a flexible PE which is allowed to bend. The rodlike PE model cannot change its conformation during simulations.

In both models, NPs are represented as impenetrable and solvent excluded spheres with a constant radius set to $R_{np} = 35.7$ Å. A positive charge z_{np} is assumed to be concentrated into a point located on their centers. In such conditions, the central point charge z_{np} of a NP mimics a constant surface charge

TABLE 1: List of Symbols

α	degree of ionization
β^c	charge ratio (the polyelectrolyte is the central element)
C_i	ionic concentration
ΔpK	difference between the apparent and intrinsic dissociation constants
γ^c	charge ratio (the nanoparticle is the central element)
N_m	number of monomers
N_{np}^{ads}	number of adsorbed nanoparticles
N_{np}^{sat}	max number of adsorbed nanoparticles since the PE is saturated
N_{np}^{box}	total number of available nanoparticles present in the simulation box
NP	nanoparticle
PE	polyelectrolyte
pH	negative logarithmic measure of hydrogen ion concentration
pK_0	negative logarithm of the intrinsic dissociation constant
$\langle R_G^2 \rangle$	mean-square radius of gyration
R_m	radius of a monomer
R_{np}	radius of a nanoparticle
σ	surface charge density of the nanoparticles
ξ	energy of interaction between the adsorbed nanoparticles and the PE, normalized by N_{np}^{ads}

density equal to $\sigma = +z_{np}$ mC/m^2. In a given simulation, all the NPs bear the same σ value. The total number of NPs present in the simulation box is noted N_{np}^{box} (Table 1). NPs are initially randomly placed in the simulation box. N_{np}^{box} is varying from 0 to 20, and four different values of NP surface charge density are considered and adjusted to $\sigma = +10, +25, +50,$ and $+100$ mC/m^2. It should be noted that the dielectric permittivity is constant throughout the system and hence surface polarization is neglected.[2,61] Monomers are considered in contact with the NP when the NP/monomer center-to-center distance is less than $R_{np} + 2R_m$. The number of adsorbed NPs is noted as N_{np}^{ads} whereas the *maximum* value of N_{np}^{ads} is noted N_{np}^{sat} since the PE is saturated (Table 1). It is thus expected that N_{np}^{sat} is found when the chain degree of ionization is equal to 1.00.

All pairs of charged particles ij interact with each other via a screened and extended version of the Debye−Hückel potential[62]

$$u_{el}(r_{ij}) = \frac{z_i z_j e^2}{4\pi \epsilon_r \epsilon_0 r_{ij} k_B T} \frac{\exp[-\kappa(r_{ij} - (R_i + R_j))]}{(1 + \kappa R_i)(1 + \kappa R_j)} \quad (4)$$

where e is the elementary charge, R is the radius of the spherical particle (monomer or NP), z is the amount of charge, ϵ_0 is the permittivity of the vacuum, k_B the Boltzmann constant, and T the temperature. Water is treated as a dielectric medium with a relative permittivity $\epsilon_r = 78.5$ at $T = 298$ K. The influence of the ionic concentration C_i is described through the Debye screening length κ^{-1}. Seven different concentrations of added salt in the range of $C_i = 0.001-0.1$ M are considered.

We performed Monte Carlo simulations according to the Metropolis algorithm.[63] The Monte Carlo simulations consist of an equilibration period followed by a production period in which data are saved every 5000 Monte Carlo steps. The multiplicity of conformations and possible dense structure formation when more than one NP are adsorbed onto a flexible or semiflexible PE chain leads in some conditions to nonreproducible results. Hence, to improve convergence to the global minimum, we used simulated annealing (SA).

SA is an optimization method applicable to search for the total energy global minimum[64] and is a technique widely used in many areas; e.g., the temperature of a molten substance is often slowly reduced until the material crystallizes to give a crystal with a minimum number of defects. A perfect crystal is thus obtained when the global minimum of the free energy is reached. In SA, at high temperature, the system is able to sample high energy regions of the conformational space and to pass over high energy barriers. Slow cooling gives then a better probability to reach the lower energy state in accordance with the Boltzmann distribution.

When model 2 is considered, the annealing schedule $T_i = f(T_{i-1})$ is used during the equilibration period where T_i is the temperature of the systems in the ith annealing step. The scaling factor f is set to $f = 0.9$, and the desired final temperature $T_f = 298$ K is reached after 40 annealing steps. When a rodlike PE is considered (model 1), the chain monomer positions are not modified during simulations. Dense structures are not achieved, and thus the simulated annealing (SA) is not necessary. As a result, the equilibration period is reduced to a unique period where $T = 298$ K. At a given temperature, successive trial chain conformations and NPs translations are generated to derive a reasonable sampling of lowest total energy on the conformational space. The monomer positions in model 2 are randomly modified by specific movements to generate new conformations: end-bond, kink-jump, and pivot. After each elementary

Nanoparticle Adsorption on a Polyelectrolyte

J. Phys. Chem. B, Vol. 110, No. 42, 2006 **20957**

random move and each NP translation, the change in energy ΔE is considered and the Metropolis selection criterion is employed to either select or reject the movement.

At a given number of Monte Carlo steps, a monomer is chosen at random and its charge state can be switched on or off respectively depending on the solution pH. According to the Metropolis Monte Carlo criteria, the energy change, ΔE, determines the probability for accepting the new charge state with

$$\Delta E = \Delta E_c \pm k_B T (\text{pH} - \text{p}K_0) \ln(10) \quad (5)$$

ΔE is the sum of the change in electrostatic interaction, ΔE_c, and the change in free energy of the intrinsic association reaction of a monomer. The minus sign is used in eq 5 when a monomer is deprotonated, whereas the plus sign is required when the monomer is protonated. In the grand canonical ensemble, the chemical potential is fixed; hence the difference pH − pK_0 is an input parameter and the degree of ionization α is measured over the production period and expressed with two significant digits. When $\alpha \geq 0.995$, the value will be noted $\alpha = 1.00$ and the chain is termed as fully charged. On the other hand, when $\alpha < 0.005$, the degree of ionization is noted as $\alpha = 0.00$ and the polymer is termed as fully uncharged.

When the PE is considered as the central entity, the charge ratio β^c is defined using a notation consistent with refs 54−56 as

$$\beta^c \equiv \left| \frac{N_{np}^{ads} z_{np}}{\alpha N_m z_m} \right| \quad (6)$$

On the other hand, considering the NP as the central entity, the charge ratio γ^c is defined as

$$\gamma^c \equiv \left| \frac{N_{train} z_m}{N_{np}^{ads} z_{np}} \right| \quad (7)$$

where N_{train} represents the number of charged monomers in trains.

It should be noted here that N_{np}^{sat} is independent of the total number of available NPs when $N_{np}^{box} \geq N_{np}^{sat}$ (as shown later in Figure 8a). The use of SA methods when flexible chains are studied requires very long CPU times. As simulation duration depends of N_{np}^{box} in a preliminary work (not reported here) the most effective N_{np}^{box} value was calculated so that no noticeable change in adsorption upon addition of more NPs than N_{np}^{sat} was observed. It explains why the maximum value of N_{np}^{box} was set to 20 and 16 when rodlike and flexible PEs are respectively considered.

III. Simulated Annealing

When one nanoparticle (NP) is considered, the sampling method used in refs 8 and 9 leads to satisfactory and reproducible results which are in good agreement with theory and experiments. Nonetheless, as mentioned in ref 9 when a semiflexible PE with one nanoparticle is considered, multiple minima problems can be encountered in particular conditions.

The multiplicity of conformations and possible dense structures when more than one NP are adsorbed onto a flexible or semiflexible PE chain is expected to lead to nonreproducible results. These results are largely dependent of the particle and monomer positions, particularly when high potentials are
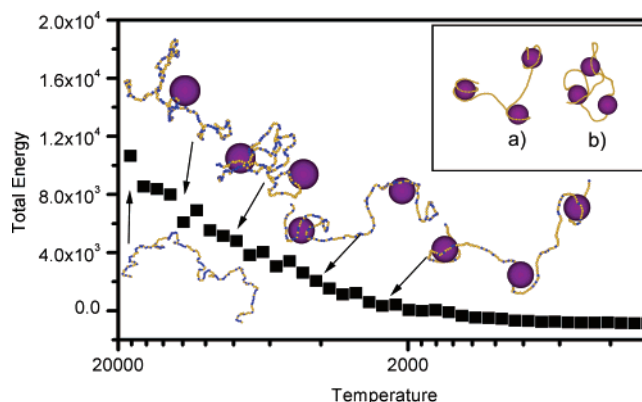

Figure 2. Variation of the system total energy as a function of temperature. The pH − pK_0 is set to 3.25 and the ionic concentration to $C_i = 0.001$ M. A semirigid PE is considered ($k_{ang} = 0.02 k_B T/\text{deg}^2$). The total number of nanoparticles in the simulation box is equal to 16 and the nanoparticle surface charge density $\sigma = +100$ mC/m^2. The final conformation (a) resulting from the production period of a simulated annealing simulation is presented in the inset. The (b) conformation is obtained without the simulated annealed technique. Nonadsorbed nanoparticles are not represented. Simulated annealing is expected to improve the production of equilibrated conformations.

involved, i.e., at high NP surface charge density or low ionic concentration regimes. In such conditions, dense complex structures are rapidly entrapped in frozen conformations.

To check the efficiency of the SA optimization method, simulations involving a semirigid PE ($k_{ang} = 0.02 \, k_B T/\text{deg}^2$) in the presence of several NPs are investigated here. To take into account intrinsic chain stiffness so as to produce solenoid structures, a bending energy is added to the flexible model 2 (see ref 9 for details). The pH − pK_0 is set to 3.25 to achieve a degree of ionization $\alpha = 1.00$ at $T_f = 298$ K. The ionic concentration is set to $C_i = 0.001$ M and the total number of NPs of surface charge density $\sigma = +100$ mC/m^2 present in the simulation box is set to $N_{np}^{box} = 16$. The variation of the total energy as a function of the temperature during the equilibration period of a given simulation is presented in Figure 2 in which some representative conformations at arbitrarily chosen temperature are depicted. Complexation is not observed at high temperature,[36] and the degree of ionization is different from $\alpha = 1.00$ due to the high energy state of the system. Then, by cooling the system, a first NP is adsorbed onto the central part of the PE. By further decrease of the temperature, a second and finally a third NP are adsorbed. It should be noted that the PE becomes more rigid as the temperature decreases. The final conformation when $T_f = 298$ and $\alpha = 1.00$ is presented in the inset of Figure 2a). The PE adopts solenoid conformations as those predicted by the analytical model of Nguyen and Shkloskii.[40,41] Such a conformation looks similar, in a qualitative way, to the DNA/histone complexes. The total energy reaches a mean value of $E_{tot} = -840 k_B T$. Such a simulation and characteristic structures are only reproducible using the SA method.

The resulting conformation in Figure 2b without SA optimization is (i) different and (ii) clearly depending on the initial distribution of the PE and the NPs in the simulation box. It should be noted that in such conditions, the number of adsorbed NPs can vary from one simulation to another, and the total energy of the presented conformation is $-310 k_B T$, demonstrating clearly that the SA method rises to conformation with lower total energy.
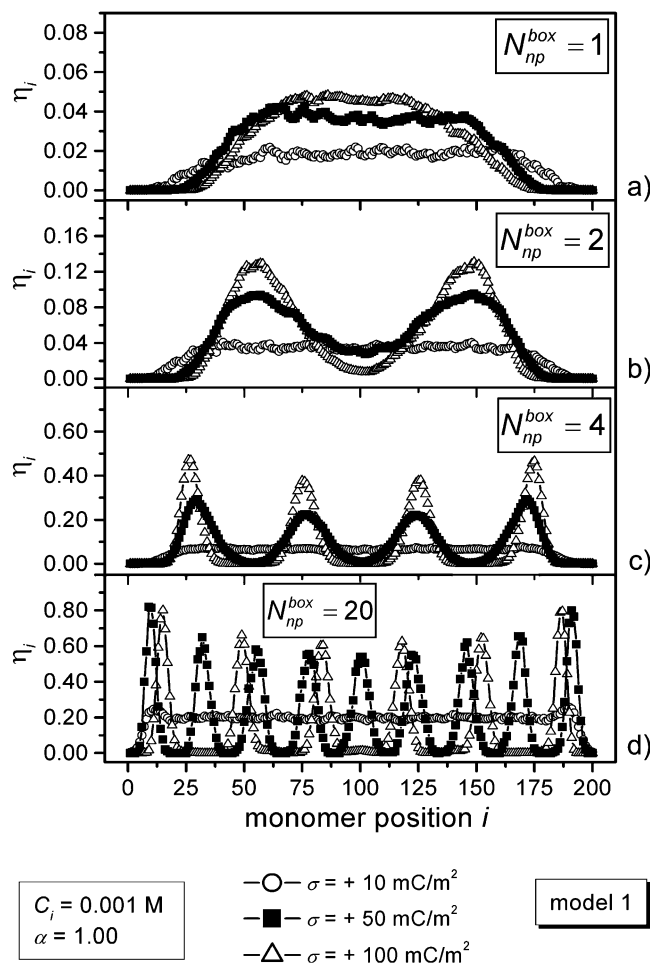
20958 *J. Phys. Chem. B, Vol. 110, No. 42, 2006*

Ulrich et al.

Figure 3. Variation of the probability of occupation of monomer i, η_i, as a function of the monomer position i for the fully charged rodlike polyelectrolyte. The number of nanoparticles present in the system is successively set to (a) $N_{np}^{box} = 1$, (b) $N_{np}^{box} = 2$, (c) $N_{np}^{box} = 4$, and (d) $N_{np}^{box} = 20$. Three different values of surface charge densities are considered at $\sigma = +10$, $+50$, and $+100$ mC/m^2 at ionic concentration $C_i = 0.001$ M. Solution conditions and NP properties control both the number of adsorbed NPs and distance correlation.

IV. Results and Discussion

Nanoparticle Distribution along the Polyelectrolyte Backbone. A subtle balance between attractive interactions and repulsions due to monomer/monomer and nanoparticle/nanoparticle interactions is expected to control the total number of adsorbed NPs as well as their distribution along the PE backbone. To determine the favorite binding regions, we defined a parameter η_i as the ratio of the number of times a monomer i is in contact with a NP over the number of MC steps of the production period. When a monomer i displays a η_i value close to 0, the monomer is almost never complexed; on the other hand when η_i goes to 1, the monomer i has a strong affinity with the NPs. A rodlike PE is investigated here to cancel the contribution of the PE conformational changes on the number and position of the adsorbed NPs.

Figure 3 displays the variation of η_i as a function of the monomer positions i for different values of the number of NPs present in the simulation box N_{np}^{box} and values of surface charge densities σ. $C_i = 0.001$ M, and pH $-$ pK_0 is large enough here to impose $\alpha = 1.00$.

When $N_{np}^{box} = 1$, the NP is adsorbed onto the central part of rodlike PE (Figure 3a). η_i values are close to zero at the chain extremities since the PE finite size effect forces

the NP to adsorb the central part of the rodlike PE to promote the electrostatic affinity between the NP and PE. This effect is more pronounced when $\sigma = +100$ mC/m^2: η_i function starts to increase when $i \approx 25$ and reaches a plateau value when $i \approx 75$.

Geometrically, according to our model description, an adsorbed NP on a rigid rod is in contact with $N_{train} \approx 4.6$ monomers. When the NPs are strongly adsorbed during a production period, then $\int_{i=1}^{200} \eta_i \approx N_{np}^{ads} N_{train}$. This condition is achieved when $\sigma = +100$ and $\sigma = +50$ mC/m^2, whereas when $\sigma = +10$ mC/m^2, $\int_{i=1}^{200} \eta_i \ll N_{np}^{ads} N_{train}$. Hence when $\sigma = +10$ mC/m^2, the NP is reversibly adsorbed and desorbed during the production period.

When more than one NP are considered, regular distances between the NPs are imposed by the electrostatic repulsions. When $N_{np}^{box} = 2$ (Figure 3b), a subtle balance emerges from NP repulsion and finite size effect; the formation of peaks instead of a plateau is now achieved. η_i function clearly provides two maxima and the central part of the rodlike PE displays here a minimum when $\sigma = +50$ and $+100$ mC/m^2. When $\sigma = +10$ mC/m^2, plateau formation demonstrates that the electrostatic repulsions between the NPs are not relevant, i.e., not strong enough to promote the formation of specific binding site. Hence, the adsorption probability function is uniform and decreases close to the PE ends.

When $N_{np}^{box} = 4$ (Figure 3c), the behavior is analogous to the previous case: a plateau is observed when $\sigma = +10$ mC/m^2 whereas four peaks are clearly obtained when $\sigma = +50$ and $+100$ mC/m^2. It should be noted, when the peaks are close to PE extremities, their amplitude is larger whereas their width is smaller. The shape of the peaks reflects the balance between (i) finite size effect which forces a NP to join the central part of the chain and (ii) NP electrostatic repulsion which promotes desorption and large separation distances between the NPs.

When $N_{np}^{box} = 20$ (Figure 3d), six and nine peaks are observed when $\sigma = +100$ and $\sigma = +50$ mC/m^2, respectively. Under such conditions, N_{np}^{box} is larger than N_{np}^{ads} and N_{np}^{ads} reaches its maximum value and is noted as N_{np}^{sat} since the PE is saturated. When $\sigma = +10$ mC/m^2, a large plateau is still observed; nonetheless, two peaks start to emerge at extremities because of finite size effect and the repulsions of the large amount of adsorbed NPs. Snapshots of the rodlike PE/NP complexes are given in Table 2a) as a function of σ and C_i when $\alpha = 1.00$. The influence of the electrostatic repulsions between the adsorbed NPs, at high σ and low C_i, clearly results in the emergence of correlation lengths between the adsorbed NPs.

The mobility and possible desorption of NPs between different adsorption sites are investigated in Figure 4 by considering the adsorption probability function for a given particle j. $\eta_{i,j}$ is defined as the η_i function of the jth NP. When $\sigma = +50$ mC/m^2 (Figure 4a), nine NPs are adsorbed onto the rodlike PE and, for the given simulation here, j values are equal to 2, 6, 9, 10, 13, 15, 17, 18, and 19. Once adsorbed, no desorption and no position exchange between adsorbed NPs are observed. On the other hand, by decreasing the surface charge densities at $\sigma = +10$ mC/m^2, a given NP can freely adsorb any monomer or desorb the PE. In Figure 4b), the $\eta_{i,j}$ function indicates that there are no specific adsorption and correlation lengths between the NPs. In addition, all the NPs in the simulation box are able to adsorb the rodlike PE.

Maximum Number of Adsorbed Nanoparticles. The value of adsorbed NPs when the PE is saturated, N_{np}^{sat}, is expected to depend on the NP surface charge density (Figure 3d), ionic

Nanoparticle Adsorption on a Polyelectrolyte

J. Phys. Chem. B, Vol. 110, No. 42, 2006 **20959**

TABLE 2: Equilibrated Conformations of (a) a Rodlike and (b) Flexible Polyelectrolyte at α = 1.00 in the Presence of Nanoparticles vs Ionic Concentration C_i[a]

a)

b)

[a] Four surface charge densities $\sigma = +10, +25, +50,$ and $+100$ mC/m^2 were considered. The nonadsorbed nanoparticles are not presented.

a)

b)
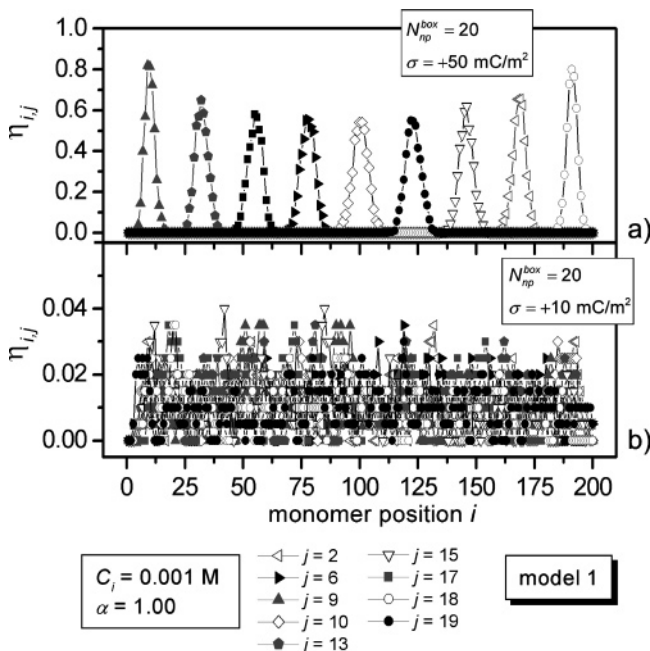
Figure 4. Variation of the probability of occupation rate of monomer i by a nanoparticle j, $\eta_{i,j}$, as a function of monomer position i. Here 9 NPs have been considered only among the 20 NPs which were present in the simulation box. When (a) $\sigma = +50$ mC/m^2, the adsorbed NPs never desorb the rodlike polyelectrolyte. When (b) $\sigma = +10$ mC/m^2, the $\eta_{i,j}$ function indicates that there are no specific adsorption regions.

concentration C_i, and solution pH. The total number of available NPs, N_{np}^{box}, was set to 20 and 16 in model 1 and model 2, respectively, to ensure $N_{np}^{box} > N_{np}^{sat}$. The variation of the mean

a)

b)
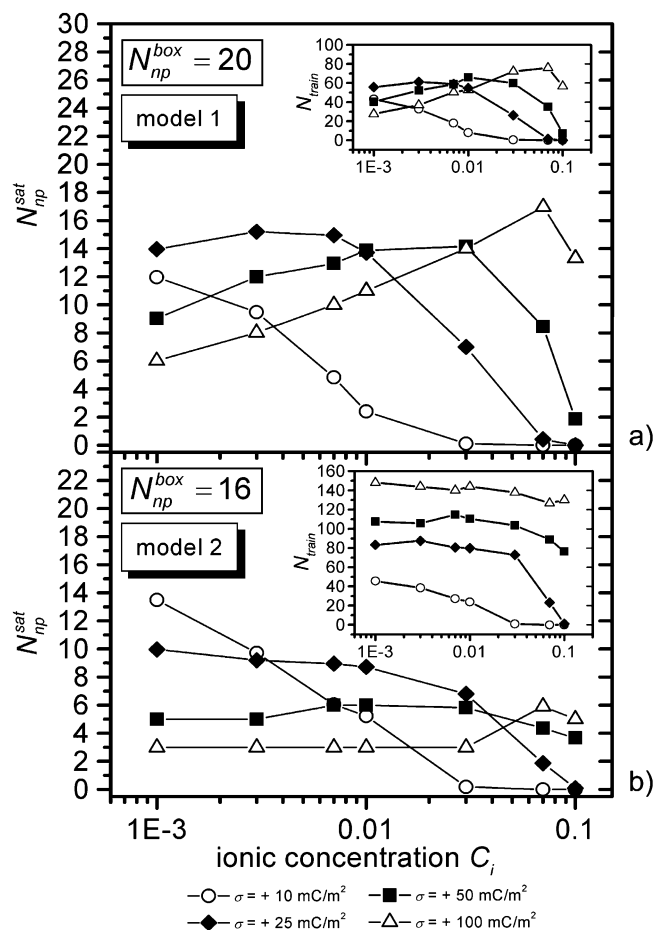
Figure 5. Variation of the maximum number of adsorbed NPs at polyelectrolyte saturation N_{np}^{sat} as a function of the ionic concentration C_i by considering (a) rodlike and (b) flexible polyelectrolytes. The variation of number of charged monomer in trains N_{train} as a function of the ionic concentration is given in the insets. Ionic centration, nanoparticle surface charge density, and polyelectrolyte flexibility are controlling in a nonmonotonic way N_{np}^{sat}.

value of N_{np}^{sat} as a function of the ionic concentration is displayed in Figure 5 when *fully charged* (α = 1.00) (a) rodlike and (b) flexible PEs are considered.

According to Figure 5a N_{np}^{sat} is clearly dependent on the surface charge density σ and ionic concentration C_i. When $\sigma = +10$ mC/m^2, the monomer/NP electrostatic attraction is mainly controlling N_{np}^{sat} which decreases as C_i increases because of electrostatic screening. As a result, the complex continuously dissolves with the increase of the ionic concentration. When $\sigma = +100$ mC/m^2, N_{np}^{sat} is increasing first as a function of the ionic concentration up to $C_i = 0.07$ M because of the increase of the electrostatic screening between the NPs. Then by furthermore increasing the ionic concentration, the complex starts to dissolve because of the decrease of the attractive interaction between the NPs and PE. Maxima are observed at intermediate surface charge density and shifted to lower ionic concentration with the decrease of σ.

The variations of the number of charged monomers in contact with the NPs are presented as a function of C_i in the inset of Figure 5a. Trends are similar to the variations of the maximum number of adsorbed NPs since the number of monomers in the train is directly calculated from the number of adsorbed NPs.

When flexible PEs are considered (model 2), and since conformational changes are expected to occur, Figure 5b shows that N_{np}^{sat} is significantly less than that obtained in the rodlike
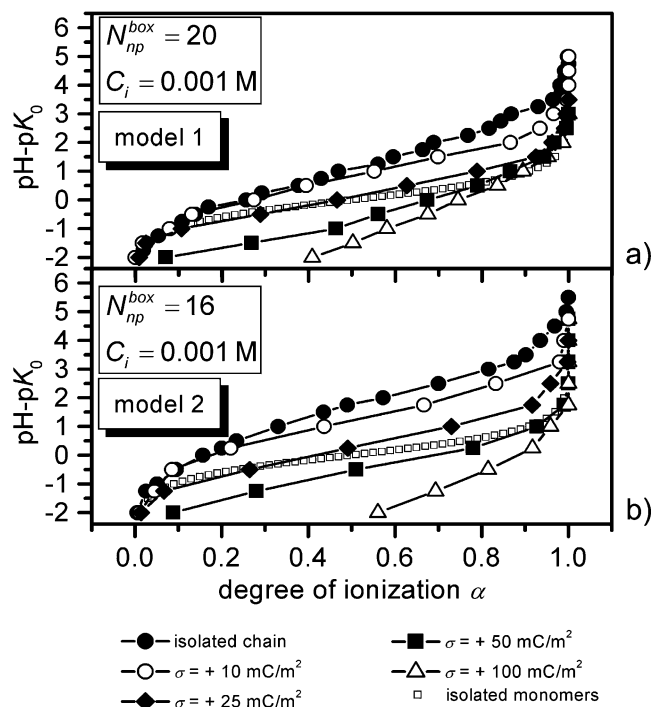
Figure 6. Titration curves corresponding to the variation of the polyelectrolyte degree of ionization α for different $pH - pK_0$. The number of NPs is set to (a) $N_{np}^{box} = 20$ in model 1 and (b) $N_{np}^{box} = 16$ in model 2. Four different surface charge densities σ (+10, +25, +50, and +100 mC/m^2) are considered at $C_i = 0.001$ M. The isolated chain titration curve is given as a reference. For a given $pH - pK_0$ value, the presence of an oppositely charged NP makes the polyelectrolyte chain easier to deprotonate. When an highly charged NP is adsorbed, the polyelectrolyte monomers become more acid than the isolated monomers.

PE case, in particular when the NP charge density $\sigma \geq +25$ mC/m^2. When $\sigma = +10$ mC/m^2, surprisingly more NPs are adsorbed on the PE. In such a case of weak adsorption conditions, PE flexibility promotes the NP adsorption by increasing the number of monomers in contact with the NPs. As shown in Table 2, dense complexes are achieved with flexible PEs which act as a polymeric glue for the NPs, resulting in an increase of the number of monomers in contact with the NPs. A balance between the total number of charged monomers in contact with the NPs, number of NPs in the complex, and complex density is then achieved. As shown in the inset of Figure 5b, when flexible PEs are considered, N_{train} is strongly dependent on the NP surface charge density. Indeed, the mean value of N_{train} for an adsorbed NP is found more important for the highly charged NPs.

Titration Curves and Complex Dissolution. Isolated titration curves of weak flexible and semiflexible PEs were previously examined in refs 8 and 9. It was shown that (i) conformational changes are obtained when α is adjusted (the chain expand continuously from $\alpha = 0.00$ to $\alpha = 1.00$) and (ii) ΔpK increases continuously with α and with the decrease of the ionic concentration. To investigate the acid/base behavior of a PE on which NPs are adsorbed, titration curves of model 1 and model 2 were calculated (parts a and b of Figure 6, respectively). The ionic concentration is set to $C_i = 0.001$ M for the sake of clarity and to highlight electrostatic effects.

As demonstrated in Figure 6, when NPs are adsorbed onto the PE, titration curves differ from the titration of the isolated chain: at a given $pH - pK_0$ value, α increases with the NP surface charge density σ, and at a given α, a decrease of the
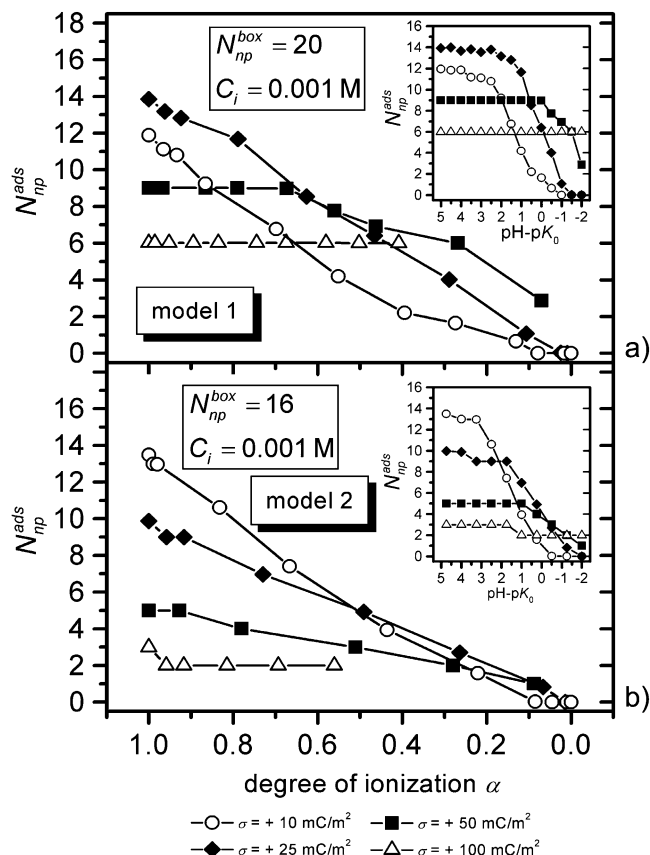
Figure 7. Variation of the number of adsorbed nanoparticles N_{np}^{ads} onto (a) a rodlike polyelectrolyte and (b) a flexible polyelectrolyte as a function of the polyelectrolyte degree of ionization α. Four different NP surface charge densities σ (+10, +25, +50, and +100 mC/m^2) were considered at a constant ionic concentration $C_i = 0.001$ M. The variations of the number of complexed nanoparticles as a function of the $pH - pK_0$ are given in the inset. Continuous decrease of N_{np}^{ads} is generally observed with decreasing the $pH - pK_0$ excepted when highly charged nanoparticles are considered (N_{np}^{ads} levels off).

ΔpK value is observed when σ increases. It should be noted that when highly charged NPs are considered ($\sigma \geq +50$ mC/m^2), the acid/base properties of the weak PE are profoundly modified since ΔpK becomes negative.

Chain stiffness influence on acid/base properties of the weak PE is clearly illustrated when titration curves of model 1 and model 2 are compared. Chain stiffness yields two effects: (i) it promotes PE ionization by increasing the chain extension hence decreasing the monomer/monomer electrostatic repulsions and (ii) it controls the number of monomers in contact with the NPs. Clearly two trends are observed. When highly charged NPs are considered, chain rigidity promotes PE ionization since the number of adsorbed NPs is important. On the other hand when weakly charged NPs are used, chain flexibility promotes PE ionization since the number of adsorbed NPs is higher than that for the rodlike PE model.

The number of adsorbed NPs, N_{np}^{ads} as a function of the PE degree of ionization α is now presented in Figure 7 for the two models. N_{np}^{ads} has the maximum value when $\alpha = 1.00$ in all conditions. When the rodlike PE is considered and $\sigma \leq +25$ mC/m^2 (Figure 7a), N_{np}^{ads} decreases monotically by decreasing α, whereas when $\sigma = +100$ mC/m^2, N_{np}^{ads} does not vary during titration and dissolution is not observed in the investigated range of $pH - pK_0$.

The distinction between two types of complexes is thus proposed: (i) *strong complexes* when the total number of

Nanoparticle Adsorption on a Polyelectrolyte

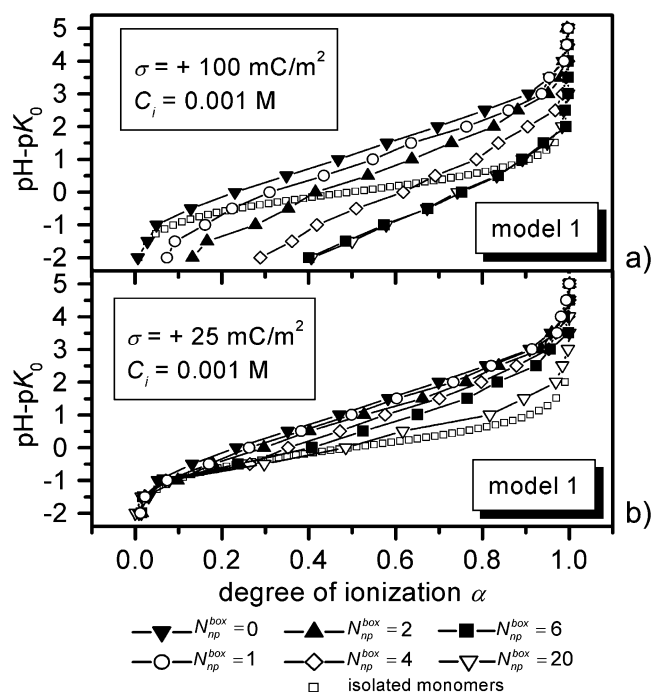*J. Phys. Chem. B, Vol. 110, No. 42, 2006* **20961**

a)

b)

Figure 8. Titration curves of a rodlike polyelectrolyte by adjusting N_{np}^{box}. The number of NPs in the simulation box is set to $N_{np}^{box} = 0, 1, 2, 4, 6$, and 20. The surface charge density σ is set to $+100$ in (a) and $+25$ mC/m^2 in (b) and the ionic concentration to $C_i = 0.001$ M. Important deviations form the isolated polyelectrolyte case are observed by increasing N_{np}^{box} and σ.

adsorbed NPs is independent over a wide range of pH (as illustrated when $\sigma = +100$ mC/m^2 and $C_i = 0.001$ M) and (ii) *weak complexes* when N_{np}^{ads} is directly controlled by the pH (as illustrated when $\sigma \leq +25$ mC/m^2 and $C_i = 0.001$ M). When $\sigma = +50$ mC/m^2, the variation of N_{np}^{ads} as a function of α displays a plateau value. When $\alpha \geq 0.65$ (strong complex regime), then, at lower α values, the complex dissolves in a monotone way (weak complex regime).

The variations of N_{np}^{ads} as a function of pH $-$ pK_0 are presented in the insets of Figure 7. Curves level off at high pH $-$ pK_0 values before smoothly decreasing at given pH $-$ pK_0 values which are dependent on NPs surface charges densities.

When a flexible PE (model 2) is considered instead of a rodlike polymer (Figure 7 b), strong and weak complex regimes are also observed. However, by comparison of the two models, dissolution is achieved at higher pH $-$ pK_0 values for the flexible chain.

To determine how the titration curves of the rodlike PE are sensible to the number of adsorbed NPs, the PE degree of ionization was calculated by varying both σ and N_{np}^{box} with N_{np}^{box} ranging from 0 to 20. Titration curves with $\sigma = +100$ mC/m^2 (strong complex) and $\sigma = +25$ mC/m^2 (weak complex) are presented in Figure 8).

When pH $-$ p$K_0 = -2$ and $N_{np}^{box} = 0$, the PE is uncharged. When one NP with $\sigma = +100$ mC/m^2 is introduced into the system, it adsorbs the PE and its degree of ionization increases to $\alpha = 0.07$. The presence of one NP induces the ionization of 14 monomers on average. By adding two, four, and six NPs into the system, α increases linearly to $2 \times 0.07 = 0.14$, $4 \times 0.07 = 0.28$, and $6 \times 0.07 = 0.42$, respectively, i.e., the number of adsorbed NPs times 0.07. This linear dependence is due to the significant separation distance between the adsorbed NPs which is greater than 14 monomers. When $N_{np}^{box} = 20$, the corresponding titration curve is identical to $N_{np}^{box} = 6$ since N_{np}^{box}
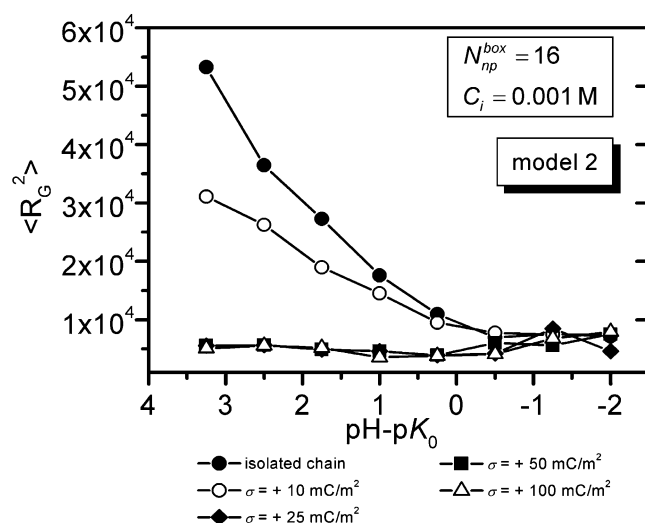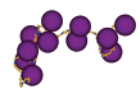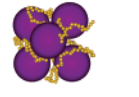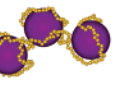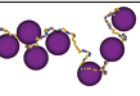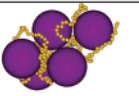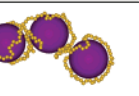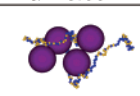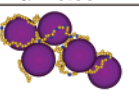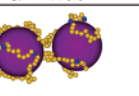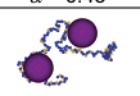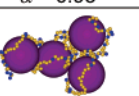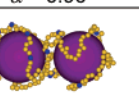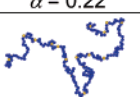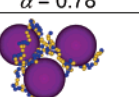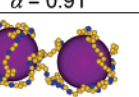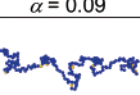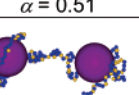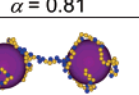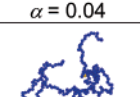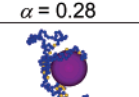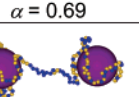

Figure 9. Variation of the mean-square radius of gyration $\langle R_G^2 \rangle$ of a flexible polyelectrolyte as a function of pH $-$ pK_0. Ionic concentration is set to $C_i = 0.001$ M. Five cases are considered: the isolated chain, then the polyelectrolyte in the presence of 16 NPs with $\sigma = +10, 25, 50$, and 100 mC/m^2. Under such conditions, complexation is observed and involves a collapse of the polyelectrolyte. Complexation results in the formation of dense conformations which are dependent on the nanoparticle surface charge density and number of adsorbed NPs. Nanoparticle desorption at small pH $-$ pK_0 values results in a small decrease of the polyelectrolyte compacity.

$= 6$. When $\sigma = +25$ mC/m^2 (weak complex, Figure 8b), the increase of N_{np}^{ads} moves the titration curves to the isolated monomers curve, the NP charge density being not high enough to achieve negative ΔpK values.

Complex Conformations of the Flexible Polyelectrolyte. When flexible PEs are considered, as shown in Tables 2b and 3, collapsed structures are obtained with a variable number of NPs. The mean-square radius of gyration $\langle R_G^2 \rangle$ of the PE is calculated to quantitatively characterize flexible PE conformational changes upon complexation or during the decrease of pH $-$ pK_0. $\langle R_G^2 \rangle$ is presented in Figure 9 as a function of pH $-$ pK_0 when $C_i = 0.001$ M for an isolated chain, then with the presence of 16 NPs with $\sigma = +10, 25, 50$, and 100 mC/m^2. When an isolated chain is considered, $\langle R_G^2 \rangle$ values are representative of extended conformations and, by decreasing the pH $-$ pK_0 value, a continuous decrease of $\langle R_G^2 \rangle$ is observed. The formation of self-avoiding walk conformations (SAW) at pH $-$ p$K_0 = -2$, i.e., at $\alpha = 0.00$, is achieved. When 16 NPs with $\sigma = +10$ mC/m^2 are included in the simulation box, a decrease of the PE $\langle R_G^2 \rangle$ is observed because of complexation and decrease of the PE charge density. $\langle R_G^2 \rangle$ decreases continuously as the pH $-$ pK_0 is decreasing and reaches the curve of the isolated chain when pH $-$ p$K_0 \leq -0.25$. Increasing further the surface charge density of the NPs, formation of more compact structures is immediately achieved. Despite the decrease of the number of adsorbed NPs during titration, $\langle R_G^2 \rangle$ values do not vary significantly. Nonetheless, as shown in Table 3, when $N_{np}^{ads} = 2$, dumbbell conformations are obtained with various separation distances between the NPs. Indeed, when $\sigma = +100$ mC/m^2 and when the degree of ionization is decreased from $\alpha = 0.96$ to $\alpha = 0.56$, the distance between the two globules is increasing since N_{train} is decreased. As a result, an increase of $\langle R_G^2 \rangle$ is observed in Figure 9 when pH $-$ p$K_0 < -0.5$. When $\sigma = +50$ mC/m^2, the dumbbell conformation is achieved at pH $-$ p$K_0 = -1.25$. When pH $-$ p$K_0 = -2.00$, the complex expels one NP and the PE wraps around the remaining NP. By

TABLE 3: Monte Carlo Equilibrated Conformations of a Weak Polyelectrolyte in the Presence of 16 Nanoparticles at $C_i = 0.001$ M as a Function of pH − pK_0 and for Three Various Surface Charge Densities $\sigma = +10$, +50, and +100 MC/m² [a]

| | | σ [mC/m²] | |
	+10	+50	+100
2.50	$\alpha = 0.83$	$\alpha = 1.00$	$\alpha = 1.00$
1.75	$\alpha = 0.66$	$\alpha = 0.99$	$\alpha = 1.00$
1.00	$\alpha = 0.43$	$\alpha = 0.93$	$\alpha = 0.96$
0.25	$\alpha = 0.22$	$\alpha = 0.78$	$\alpha = 0.91$
-0.5	$\alpha = 0.09$	$\alpha = 0.51$	$\alpha = 0.81$
-1.25	$\alpha = 0.04$	$\alpha = 0.28$	$\alpha = 0.69$
-2.00	$\alpha = 0.00$	$\alpha = 0.09$	$\alpha = 0.56$

[a] The average value of the degree of ionization α is given in the inset of each cell.

furthermore decreasing the pH − pK_0 (data not reported here), the last NP desorbs and $\langle R_G^2 \rangle$ increases to the SAW value.

Overcharging. Considering the PE as the central element, a neutral complex is observed when β^c is equal to 1 (eq 6); an undercharged complex is obtained when $\beta^c < 1$ because of the excess of PE charges, whereas, when $\beta^c > 1$, the excess of NP charges involves overcharging. The variation of β^c as a function of the ionic concentration C_i is given in Figure 10 for the (a) rodlike and (b) flexible PEs when $\alpha = 1.00$. The ionic concentration has a nonlinear effect which is dependent on the NP surface charge. Considering the rodlike PE, when $\sigma = +10$ mC/m², the complex is undercharged whatever C_i and β^c decreases by increasing C_i. When $\sigma = +25$ mC/m², by increasing C_i, transitions from an overcharged PE/NP complex to a neutral complex and to an undercharged complex are observed in agreement with the observation made by Skepö and Linse.[56] When $\sigma = +50$ mC/m², the variation of β^c as a function of C_i exhibits a more subtle behavior since overcharging increases with C_i to reach a maximum value, then by increasing further C_i, a transition from an overcharged to an undercharged complex is achieved. When $\sigma = +100$ mC/m², the complex is always overcharged. However, a maximum value of β^c is observed at $C_i = 0.07$ M and a decrease of the overcharging is achieved in the high ionic concentration regime.
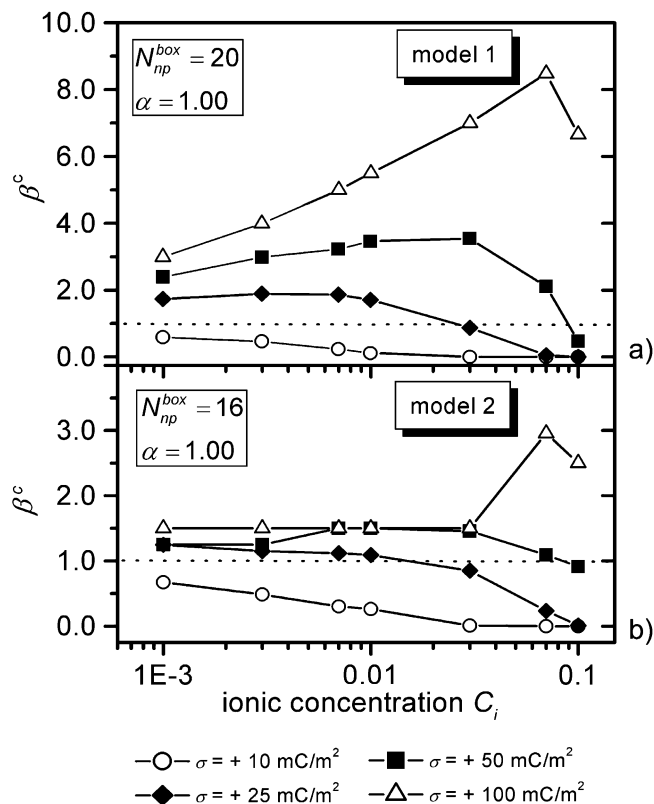

Figure 10. Variation of the charge ratio β^c of the amount of nanoparticle charge over the polyelectrolyte total charge as a function of the ionic concentration for (a) a rodlike polyelectrolyte and (b) a flexible polyelectrolyte. The polyelectrolyte overcharging is expected to be maximum for a given ionic concentration using highly charged nanoparticles. Chain rigidity is promoting here the overcharging.

Overcharging is more important for the rodlike PE and is systematically increased by increasing further the NP surface charge density σ. Trends are similar when the flexible PE is considered. However, a plateau is observed when $\sigma = +100$ mC/m² and $C_i \leq 0.03$ M due to the limited number of adsorbed NPs.

The variations of β^c as a function of pH − pK_0 are presented in Figure 11 when $C_i = 0.001$ M and for the rodlike PE model (similar trends are obtained with the flexible PE). Two trends are clearly put in evidence: when $\sigma \leq +25$ mC/m², β^c continuously decreases during titration. Transition from overcharged to undercharged and then dissolved complex is obtained. On the other hand, when $\sigma \geq +50$ mC/m², overcharging increases continuously by decreasing pH − pK_0 since the number of adsorbed NP is kept more or less constant here.

Considering now the NP as the central element, the overcharging for an adsorbed NP (eq 7) is solely achieved for a flexible PE when C_i is equal to 0.03, 0.05, or 0.07 M, $\sigma = +100$ mC/m² and $\alpha = 1.00$. In same conditions, when a rodlike PE is considered, the NP is largely undercharged.

Annealed vs Quenched Polyelectrolyte Charge Distribution. In our models, the total number of charges as well as their distribution along the PE backbone are expected to be controlled by the pH and the presence of NPs. Charges corresponding to α less than unity are subject to equilibrium and may thus be considered mobile. This effect is illustrated in Figure 12 in which charges migrate to the binding region and are depleted from locally unbound repeat monomer units.

To investigate the influence of charge mobility, a quenched PE is considered by regularly distributing the charges along the
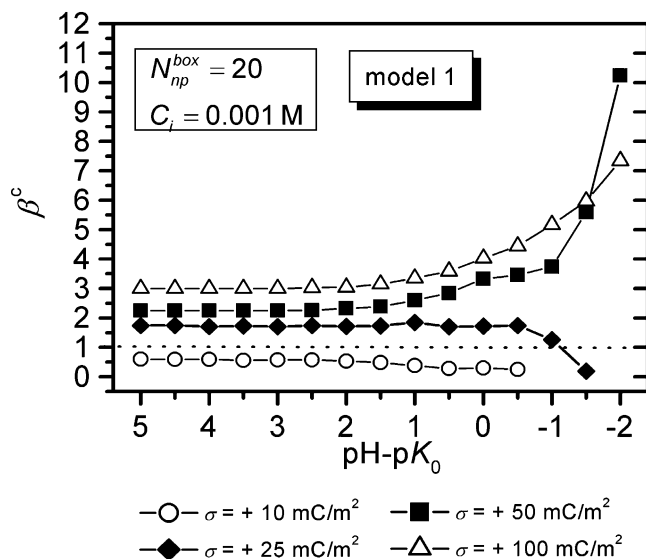
Nanoparticle Adsorption on a Polyelectrolyte

J. Phys. Chem. B, Vol. 110, No. 42, 2006 **20963**

Figure 11. Variation of the charge ratio β^c as a function of the pH − pK_0 for a rodlike polyelectrolyte. Two trends are observed with decreasing pH − pK_0 and subsequently the polyelectrolyte degree of ionization α. At low NP surface charge density σ, undercharging is observed whereas overcharging is promoted with increasing σ.
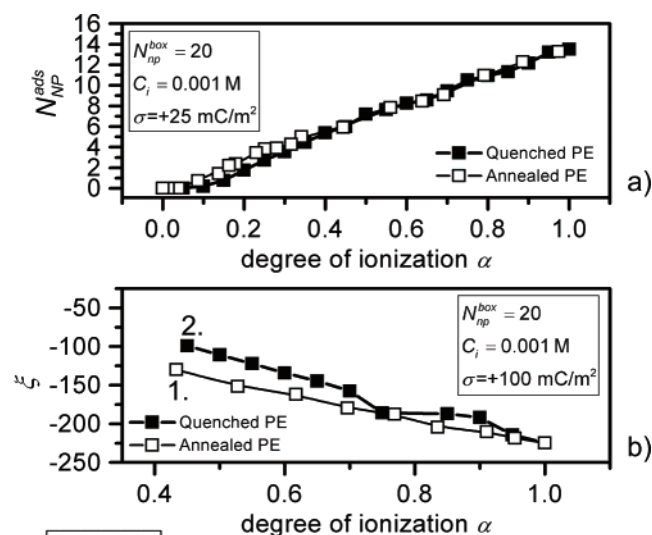

Figure 12. (a) Variation of the number of adsorbed NPs as a function of the degree of ionization for an annealed and a quenched polyelectrolyte. Charge mobility at weak polyelectrolyte degree of ionization promotes the NP adsorption. (b) Variation of the mean energy of interaction between one adsorbed NP and the polyelectrolyte, ξ, as a function of α for an annealed and a quenched polyelectrolyte. In all cases, a stronger affinity is achieved by considering annealed polyelectrolyte. Snapshots of equilibrated conformations are presented for the annealed (1) and quenched (2) polyelectrolyte.

PE backbone for different α. The variation of N_{np}^{ads} vs α is presented in Figure 12a using a rodlike PE, σ = +25 mC/m² and C_i = 0.001 M. When α > 0.40, N_{np}^{ads} is found similar on both a quenched and an annealed PE. On the other hand, when 0 < α ≤ 0.40, i.e., in unfavorable conditions for NP adsorption,

the annealed PE, due to the charge mobility, is more efficient for the NP binding.

The parameter ξ is defined as the total energy of interaction between the NPs in the simulation box and the PE, normalized by N_{np}^{ads}. The variations of ξ for the quenched and annealed rodlike PE as a function of α when C_i = 0.001 M and σ = +100 mC/m² are presented in Figure 12b. As suggested above, we demonstrate here that the annealed PE creates a strong complex (when α = 1.00, N_{np}^{ads} = 6 for both PEs). $\xi_{quenched} \geq \xi_{annealed}$ in the full α domain investigated. Considering the quenched PE, when α = 0.75, N_{np}^{ads} falls from 6 to 5 (weak complex) and as a result $\xi_{quenched} \approx \xi_{annealed}$.

V. Conclusions

This paper investigated the formation of complexes between a polyelectrolyte (PE) and oppositely charged nanoparticles (NPs) when electrostatic interactions are considered. One of the key questions was to know what happens, using Monte Carlo simulations, to the PE conformation and structure of the complexes when the solution ionic concentration, pH, NP surface charge density, and PE intrinsic rigidity were modified. We found that the key to the qualitative understanding of the *zoology* of PE/NP complexes is the balance between attractive PE/NP interactions and monomer/monomer and nanoparticle/nanoparticle repulsions, both controlled by adjusting bulk properties such as pH and ionic concentration.

Rodlike and flexible polyelectrolytes were considered, and stiffness was found to be an important parameter since flexible PEs act as polymeric glue promoting the formation of dense structures.

In the case of flexible PEs, the maximum number of adsorbed nanoparticles is significantly less than those seen in the rodlike PE case. However when NP surface charge is low, flexibility promotes NP adsorption by increasing the number of monomers in contact with the NPs. On the other hand, chain stiffness decreases the impact of monomer/monomer electrostatic repulsions by increasing the chain extension but decreases the number of monomers in contact with the NPs. In such conditions, complex conformations were characterized by considering the distance correlation between the adsorbed NP as well as the NP mobility on the rodlike PEs.

Overcharging, which is an important issue if, for example, complex aggregation should be considered, was found to be more important for the rodlike PEs and systematically increased by increasing further the NP surface charge density as well as ionic concentration (prior to NP desorption). Another important issue to promote PE/NP complex formation, which is related to the PE chemical structure, concerns the charge mobility along the PE backbone. Clearly when charge mobility is possible (annealed PE), the PE acts as a better glue for the NPs, promoting the monomer/NP attractive interaction contrary to quenched PEs.

The investigation of the titration curves of the weak PE also reveals an important change in the PE acid/base properties upon the adsorption for NPs by promoting PE ionization. The presence of several NPs makes, in some conditions, the PE easier to deprotonate than the isolated monomer.

These simulations have shown that when dense structures involving several NPs are expected to be obtained, then the use of simulated annealing is required to improve convergence to the most probable global minimum. Given to the needs to identify, understand, and monitor parameters which are related to the structure/property relationship of PE/NP mixtures and

20964 *J. Phys. Chem. B, Vol. 110, No. 42, 2006*

Ulrich et al.

structural zoology of such systems, computer simulations represent a very useful tool to quantify such systems.

References and Notes

(1) Ullner, M. Polyelectrolyte models in theory and simulation. In *Handbook of Polyelectrolytes and Their Applications*; Tripathy, S. K., Kumar, J., Nalwa, H. S., Eds.; American Scientific Publishers: Los Angeles, 2002; Vol. 3; p 271.

(2) Dobrynin, A. V.; Rubinstein, M. *Prog. Polym. Sci.* **2005**, *30*, 1049.

(3) Katchalsky, A.; Shavit, N.; Eisenberg, H. *J. Polym. Sci.* **1954**, *13*, 69.

(4) Braud, C. *Colloq. Int. C. N. R. S.* **1976**, *246*, 247.

(5) Reed, C. E.; Reed, W. F. *J. Chem. Phys.* **1992**, *96*, 1609.

(6) Raphael, E.; Joanny, J. F. *Europhys. Lett.* **1990**, *13*, 623.

(7) Ullner, M.; Woodward, C. E. *Macromolecules* **2000**, *33*, 7144.

(8) Ulrich, S.; Laguecir, A.; Stoll, S. *J. Nanopart. Res.* **2004**, *6*, 595.

(9) Ulrich, S.; Laguecir, A.; Stoll, S. *Macromolecules* **2005**, *38*, 8939.

(10) Laguecir, A.; Ulrich, S.; Labille, J.; Fatin-Rouge, N.; Stoll, S.; Buffle, J. *Eur. Polym. J.* **2006**, *42*, 1135.

(11) Meijer, E. W.; van Genderen, M. H. P. *Nature (London, U.K.)* **2003**, *426*, 128.

(12) Allen, T. M.; Cullis, P. R. *Science (Washington, DC, U.S.)* **2004**, *303*, 1818.

(13) Service Robert, F. *Science* **2004**, *304*, 1732.

(14) Kagan, V. E.; Bayir, H.; Shvedova, A. A. *Nanomedicine* **2005**, *1*, 313.

(15) Kipen Howard, M.; Laskin Debra, L. *Am. J. Physiol.: Lung Cell. Mol. Physiol.* **2005**, *289*, L696.

(16) Schwoyer, W. L. K. *Polyelectrolytes for Water and Wastewater Treatment*; CRC Press: Boca Raton, FL, 1981.

(17) Kam, S.-K.; Gregory, J. *Water Res.* **2001**, *35*, 3557.

(18) Hunkeler, D. *Spec. Chem. Mag.* **2003**, *23*, 21.

(19) Osaka, T.; Matsunaga, T.; Nakanishi, T.; Arakaki, A.; Niwa, D.; Iida, H. *Anal. Bioanal. Chem.* **2006**, *384*, 593.

(20) Berret, J.-F.; Schonbeck, N.; Gazeau, F.; El Kharrat, D.; Sandre, O.; Vacher, A.; Airiau, M. *J. Am. Chem. Soc.* **2006**, *128*, 1755.

(21) Filella, M.; Buffle, J. *Colloids Surf., A* **1993**, *73*, 255.

(22) Xia, J.; Dubin, P. L. *Macromol. Complexes Chem. Biol.* **1994**, 247.

(23) Cooper, C. L.; Dubin, P. L.; Kayitmazer, A. B.; Turksen, S. *Curr. Opin. Colloid Interface Sci.* **2005**, *10*, 52.

(24) Dubin, P. L.; The, S. S.; McQuigg, D. W.; Chew, C. H.; Gan, L. M. *Langmuir* **1989**, *5*, 89.

(25) Zhang, H. W.; Ray, J.; Manning, G. S.; Morrefield, C. N.; Newkome, G. R.; Dubin, P. L. *J. Phys. Chem. B* **1999**, *103*, 2347.

(26) Miura, N.; Dubin, P. L.; Moorefield, C. N.; Newkome, G. R. *Langmuir* **1999**, *15*, 4245.

(27) Feng, X. H.; Dubin, P. L.; Zhang, H. W.; Kirton, G. F.; Bahadur, P.; Parotte, J. *Macromolecules* **2001**, *34*, 6373.

(28) Wang, Y.; Dubin, P. L.; Zhang, H. *Langmuir* **2001**, *17*, 1670.

(29) Seyrek, E.; Dubin, P. L.; Tribet, C.; Gamble, E. A. *Biomacromolecules* **2003**, *4*, 273.

(30) Kayitmazer, A. B.; Seyrek, E.; Dubin, P. L.; Staggemeier, B. A. *J. Phys. Chem. B* **2003**, *107*, 8158.

(31) Mattison, K. W.; Dubin, P. L.; Brittain, I. J. *J. Phys. Chem. B* **1998**, *102*, 3830.

(32) Xia, J.; Dubin, P. L.; Kim, Y.; Muhoberac, B. B.; Klimkowski, V. J. *J. Phys. Chem.* **1993**, *97*, 4528.

(33) Berret, J. F.; Yokota, K.; Morvan, M. *Soft Mater.* **2004**, *2*, 71.

(34) Sehgal, A.; Lalatonne, Y.; Berret, J. F.; Morvan, M. *Langmuir* **2005**, *21*, 9359.

(35) Ilekti, P.; Martin, T.; Cabane, B.; Piculell, L. *J. Phys. Chem. B* **1999**, *103*, 9831.

(36) von Goeler, F.; Muthukumar, M. *J. Chem. Phys.* **1994**, *100*, 7796.

(37) Muthukumar, M. *Colloid-Polym. Interact.* **1999**, 175.

(38) Mateescu, E. M.; Jeppesen, C.; Pincus, P. *Europhys. Lett.* **1999**, *46*, 493.

(39) Nguyen, T. T.; Shklovskii, B. I. *J. Chem. Phys.* **2001**, *114*, 5905.

(40) Nguyen, T. T.; Grosberg, A. Y.; Shklovskii, B. I. *J. Chem. Phys.* **2000**, *113*, 1110.

(41) Nguyen, T. T.; Shklovskii, B. I. *Physica A* **2001**, *293*, 324.

(42) Netz, R. R.; Joanny, J. F. *Macromolecules* **1998**, *31*, 5123.

(43) Netz, R. R.; Joanny, J. F. *Macromolecules* **1999**, *32*, 9026.

(44) Netz, R. R.; Joanny, J.-F. *macromolecules* **1999**, *32*, 9013.

(45) Boroudjerdi, H.; Netz, R. R. *Europhys. Lett.* **2005**, *71*, 1022.

(46) Boroudjerdi, H.; Netz, R. R. *J. Phys.: Condes. Matter* **2005**, *17*, S1137.

(47) Cooper, C. L.; Goulding, A.; Kayitmazer, A. B.; Ulrich, S.; Stoll, S.; Turksen, S.; Yusa, S.-I.; Kumar, A.; Dubin, P. L. *Biomacromolecules* **2006**, *7*, 1025.

(48) Wallin, T.; Linse, P. *Langmuir* **1996**, *12*, 305.

(49) Kong, C. Y.; Muthukumar, M. *J. Chem. Phys.* **1998**, *109*, 1522.

(50) Chodanowski, P.; Stoll, S. *J. Chem. Phys.* **1999**, *111*, 6069.

(51) Chodanowski, P.; Stoll, S. *J. Chem. Phys.* **2001**, *115*, 4951.

(52) Stoll, S.; Chodanowski, P. *Macromolecules* **2002**, *35*, 9556.

(53) Akinchina, A.; Linse, P. *Macromolecules* **2002**, *35*, 5183.

(54) Jonsson, M.; Linse, P. *J. Chem. Phys.* **2001**, *115*, 3406.

(55) Jonsson, M.; Linse, P. *J. Chem. Phys.* **2001**, *115*, 10975.

(56) Skepoe, M.; Linse, P. *Phys. Rev. E: Stat., Nonlinear, Soft Matter Phys.* **2002**, *66*, 051807/1.

(57) Laguecir, A.; Stoll, S.; Kirton, G.; Dubin, P. L. *J. Phys. Chem. B* **2003**, *107*, 8056.

(58) Ballauff, M.; Blaul, J.; Guilleaume, B.; Rehahn, M.; Traser, S.; Wittemann, M.; Wittmeyer, P. *Macromol. Symp.* **2004**, *211*, 1.

(59) Buffle, J.; Wilkinson, K. J.; Stoll, S.; Filella, M.; Zhang, J. *Environ. Sci. Technol.* **1998**, *32*, 2887.

(60) Manning, G. S. *J. Chem. Phys.* **1969**, *51*, 924.

(61) Israelachvili, J. N. *Intermolecular and Surface Forces*, 2nd ed.; Academic Press: London, 1991.

(62) Verwey, E. J. W.; Overbeek, J. T. G. *Theory of the Stability of Lyophobic Colloids*; Dover: Mineola, 1999.

(63) Metropolis, N.; Rosenbluth, A. W.; Rosenbluth, M. N.; Teller, A. H.; Teller, E. *J. Chem. Phys.* **1953**, *21*, 1087.

(64) Kirkpatrick, S.; Gelatt, C. D., Jr.; Vecchi, M. P. *Science* **1983**, *220*, 671.